

Chapter 9

Supporting Information for Chapter 8

M. Murialdo, N.P. Stadie, C.C. Ahn, and B. Fultz, "A Generalized Law of Corresponding States for the Physisorption of Classical Gases with Cooperative Adsorbate-Adsorbate Interactions," *J. Phys. Chem. C*, 120, 11847 (2016).

(Supporting Information)

DOI: 10.1021/acs.jpcc.6b00289

<http://pubs.acs.org/doi/abs/10.1021/acs.jpcc.6b00289>

S1. Adsorbent Materials

MSC-30

MSC-30 (Maxsorb) is a microporous superactivated carbon obtained from Kansai Coke & Chemicals Company Ltd. (Japan). As determined by nitrogen adsorption and BET analysis, MSC-30 has a surface area of $3244 \pm 28 \text{ m}^2 \text{ g}^{-1}$. Using nitrogen adsorption data and a slit-pore model, NLDFT pore-size analysis¹ was conducted to determine the pore-size distribution. MSC-30 has a broad range of pore sizes (from 6 to 35 Å). Over 40% of the micropore volume is contained in pores of greater than 21 Å in width. The total micropore volume was found to be $1.54 \text{ cm}^3 \text{ g}^{-1}$ by the Dubinin-Radushkevich method. The skeletal density was measured by helium pycnometry and determined to be 2.1 g cm^{-3} . Cu K α X-ray diffraction of MSC-30 gave a broad peak at $2\theta=34^\circ$, in accordance with that reported for AX-21. The elemental composition (CHN) was determined via the Dumas method² in combustion experiments, indicating that 1.16 wt% of MSC-30 is hydrogen. Results from XPS experiments on MSC-30 are summarized in Table S1.³

Table S1. Summary of XPS Data on MSC-30 and ZTC

peak position (eV)	285.0	285.7	286.4	287.3	288.1	289.4	290.2	291.5
component	C-C sp ²	C-C sp ³	C-OR	C-O-C	C=O	COOR	-	-
ZTC	53.4	18.0	8.6	6.0	1.1	4.2	1.0	7.7
MSC-30	48.0	18.8	6.8	4.8	6.1	4.2	3.6	7.7

CNS-201

CNS-201 is a microporous activated carbon obtained from A. C. Carbone Inc. (Canada). As determined by nitrogen adsorption and BET analysis, CNS-201 has a surface area of $1095 \pm 8 \text{ m}^2 \text{ g}^{-1}$. Using nitrogen adsorption data and a slit-pore model, NLDFT pore-size analysis was conducted to determine the pore-size distribution. CNS-201 has a three dominant pore widths of 5.4, 8.0, and 11.8 Å, containing roughly 50%, 20%, and 15% of the total micropore volume respectively. The micropore volume was found to be $0.45 \text{ cm}^3 \text{ g}^{-1}$ by the Dubinin-Radushkevich method^{4,5}. The skeletal density was measured by helium pycnometry and determined to be 2.1 g cm^{-3} .

Zeolite-Templated Carbon (ZTC)

ZTC is a templated carbon synthesized using zeolite NaY and a process described elsewhere.^{6,7} As determined by nitrogen adsorption and BET analysis, ZTC has a surface area of $3591 \pm 60 \text{ m}^2 \text{ g}^{-1}$. Using nitrogen adsorption data and a slit-pore model, NLDFT pore-size analysis was conducted to determine the pore-size distribution. ZTC has a narrow pore-size distribution centered at 12 Å. Over 90% of the micropore volume is contained in pores of

widths between 8.5 and 20 Å. The total micropore volume was found to be 1.66 cm³ g⁻¹ by the Dubinin-Radushkevich method. The skeletal density was measured by helium pycnometry and determined to be 1.8 g cm⁻³. Cu K α X-ray diffraction of ZTC produced a sharp peak at $2\theta=6^\circ$, indicative of the template periodicity of ~ 15 Å. The elemental composition (CHN) was determined using the Dumas method in combustion experiments, indicating that 2.44 wt% of MSC-30 is hydrogen. Results from XPS experiments on ZTC are summarized in Table S1. TEM analysis has also provided evidence of the periodic structure of ZTC.³

S2. Approximation of n_{max}

All three materials tested are predominantly microporous. The maximum adsorption quantity (n_{max}) was estimated as the product of the total micropore volume and the liquid density of the adsorptive species at its triple point. This assumes complete micropore filling at a maximal density given by the liquid-phase density. The micropore volumes of each adsorbent were determined by applying the Dubinin-Radushkevich method to nitrogen adsorption isotherms measured at 77 K.³ The liquid densities were obtained from REFPROP⁸. Both the micropore volumes and the liquid densities are listed in Table S2 along with the as-determined values for n_{max} .

Table S2. Liquid Molar Densities, Adsorbent Micropore Volumes, and Estimated n_{max} Values

	density (mol dm ⁻³)	ZTC	MSC-30	CNS-201
micropore volume (cm ⁻³)		1.66	1.54	0.45
krypton	29.2	48.5	45.0	13
methane	28.1	46.7	43.3	13
ethane	21.7	36.0	33.4	9.8

S3. Comparison of Fractional Occupancies at Corresponding Conditions

While absolute adsorption is of greater physical relevance, excess adsorption is the experimentally-determined quantity in physisorption experiments. To obtain absolute adsorption uptake quantities (n_a) from excess adsorption quantities (n_e) we used Gibb's definition of excess adsorption

$$n_e = n_a - V_{ads}\rho_g \quad (S1)$$

where ρ_g is the gas-phase density. We fit the unknown absolute adsorption uptake quantities and adsorption volumes (V_{ads}) with a superposition of Langmuir isotherms⁹ to obtain

$$n_e = (n_{max} - V_{max}\rho_g) \left(\sum_i \alpha_i \left(\frac{K_i P}{1 + K_i P} \right) \right) \quad (S2)$$

where K_i is the equilibrium constant of the i th Langmuir isotherm, α_i is the weighting factor for the i th Langmuir isotherm ($\sum_i \alpha_i = 1$), and V_{max} is the maximum adsorption volume. While the number of Langmuir isotherms (i) may be adjusted, we found that setting $i=2$ gives high quality fits with a minimum number of parameters. Moreover many of the fitting parameters hold physical significance that may be verified by comparison to independent estimates. For $i=2$, the absolute adsorption is given by

$$n_a = n_{max} \left((1 - \alpha) \left(\frac{K_1 P}{1 + K_1 P} \right) + \alpha \left(\frac{K_2 P}{1 + K_2 P} \right) \right) \quad (S3)$$

This fitting procedure has been described in more detail elsewhere.⁹

Having determined absolute adsorption, we compare the fractional occupancies of methane, krypton and ethane on ZTC and MSC-30 at corresponding reduced temperatures of

1.25 \pm 0.02 and 1.38 \pm 0.03 and corresponding reduced pressures (Figure S1). CNS-201 was not considered due to an insufficient number of experimental isotherms.

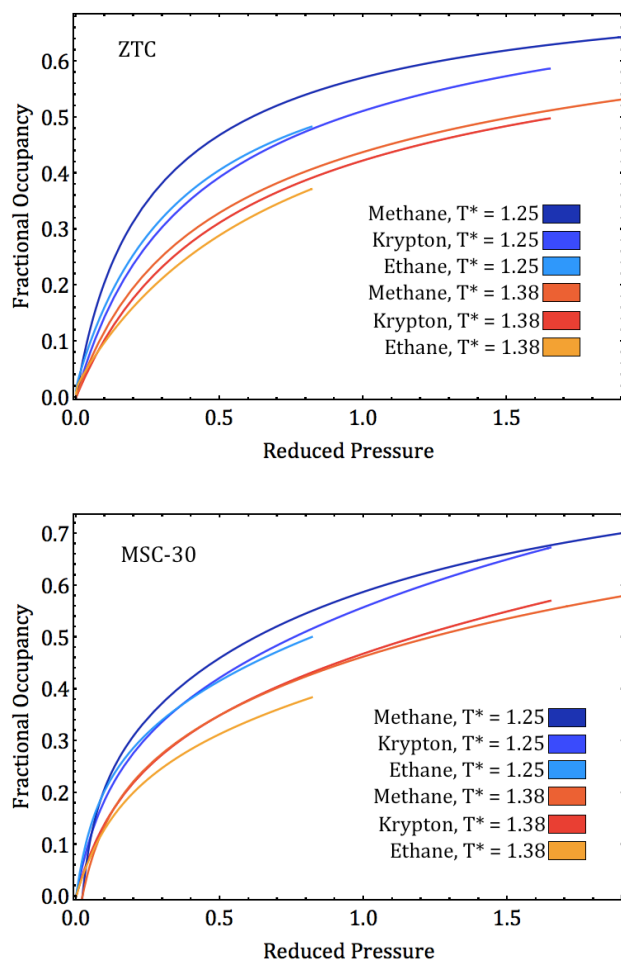


Figure S1. Comparison of krypton, methane and ethane fractional occupancies on ZTC and MSC-30 at corresponding conditions.

As with the excess occupancies, the fractional occupancies compared at corresponding conditions are in reasonable agreement with one another. Additional errors may have been introduced in the fitting procedure.

S4. Assumption that S_g (in Reference to S_{L1}) is Well Approximated by $f(T^R, P^R)$ for Monatomic Gases with Similar Critical Volumes

According to the Trouton-Hildebrand-Everett rule, “the entropy of vaporization for normal liquids is the same when evaporated to the same concentration”.¹⁰ Despite notable exceptions (e.g. due to hydrogen bonding), the Trouton-Hildebrand-Everett rule is generally accurate.^{11,12} The entropy of vaporization (ΔS_{vap}) is defined as the difference between the gas-phase entropy (S_{g1}) and the liquid-phase entropy (S_{L1}), where the “1” subscript indicates that the entropies are measured at the normal boiling temperature.

$$\Delta S_{vap} = S_{g1} - S_{L1} \quad (S4)$$

For a monatomic gas at dilute conditions, additional changes to the gas-phase enthalpy due to increasing temperature are accounted for as

$$\Delta S_{g\ 1 \rightarrow 2} = \frac{3}{2} R \ln\left(\frac{T}{T_{BP}}\right) \quad (S5)$$

where the subscript “ $g\ 1 \rightarrow 2$ ” indicates that the entropy change takes the gas from the normal boiling temperature, 1, to a new temperature, 2. Noting the proportionality between the normal boiling temperature and the critical temperature for gases with similar V_c

$$\Delta S \propto \frac{3}{2} R \ln(T^R) \quad (S6)$$

For gases with similar V_c , the gas concentration, or equivalently the molar volume (V), is approximately proportional to V^R , and the difference between S_{g2} and S_{L1} is well approximated as a function that depends only on T^R and V^R , $f(T^R, V^R)$. Figure S2 compares the gas-phase entropies (measured in reference to S_{L1}) of three monatomic gases with similar critical volumes (argon, $0.096\text{ dm}^3\text{ mol}^{-1}$; krypton $0.12\text{ dm}^3\text{ mol}^{-1}$; xenon $0.15\text{ dm}^3\text{ mol}^{-1}$) and

one monatomic gas with a different critical volume (neon, $0.051 \text{ dm}^3 \text{ mol}^{-1}$) at corresponding conditions.⁸ The gas-phase entropies of argon, krypton, and xenon are all in good agreement with one another, while that of neon deviates significantly due to its smaller critical volume and quantum effects.

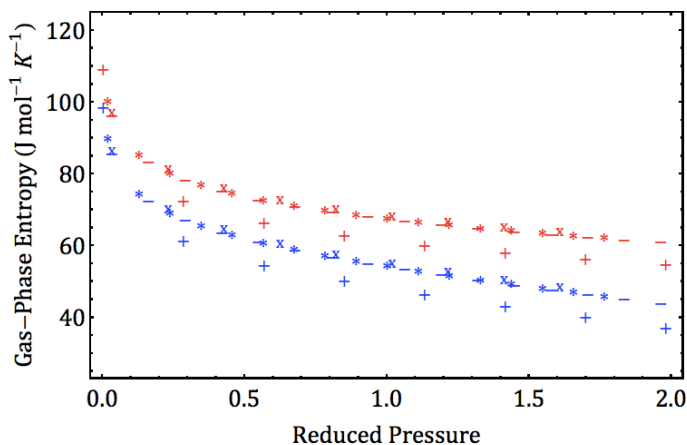


Figure S2. Gas-Phase molar entropies of neon (+), argon (-), krypton (*), and xenon (x) at reduced temperatures of 1.25 (blue) and 2.07 (red), at corresponding reduced pressures.

S5. Assumption that ΔH_{ads} is Proportional to T_c

For interactions from purely London dispersion forces, ΔH_{ads} is expected to be proportional to the static polarizability (α) of the adsorbate following London's theory¹³. This assumption is valid for small and moderately-sized classical molecules (e.g., ethane) that have a fairly uniform charge distribution (e.g., non-polar species without a strong quadrupole moment).

For small and moderately-sized classical molecules that interact through

London dispersion forces, the critical temperature is found to be proportional to the square root of the static polarizability¹⁴. In many cases, however, the curvature is minimal and the trend is essentially linear. This is illustrated for noble gases in Figure S3.

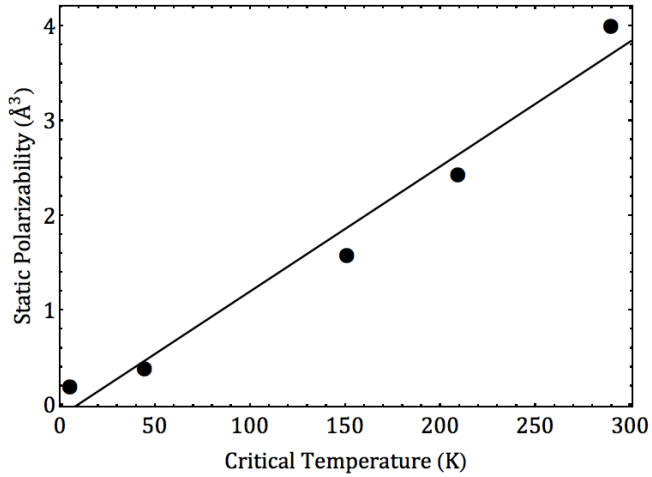


Figure S3. Static polarizability of noble gases¹⁵ as a function of the gas critical temperature⁸. A linear fit is shown.

Therefore, a simple approximation that the critical temperature is directly proportional to the polarizability (α) is acceptable:

$$\alpha \approx c_5 T_c \quad (\text{S7})$$

Here, c_5 is the proportionality constant. It then follows that:

$$\Delta H_{ads} \approx c_6 T_c \quad (\text{S8})$$

$$\frac{(\Delta H_{ads})}{T_c} \approx c_6 \quad (\text{S9})$$

The validity of this approximation is investigated in Table S3, wherein $-\Delta H_{ads}$ is derived experimentally from adsorption measurements (at $\theta \approx 0$ on ZTC, MSC-30, and CNS-201). We find that c_6 is reasonably constant across different gases on the same adsorbent. As is a

commonly employed assumption elsewhere, the effect of temperature on the isosteric enthalpy of adsorption is assumed to be negligible compared to its absolute magnitude.

Table S3. Empirical Values of $\frac{(-\Delta H_{ads})}{T_c}$ for Krypton,

Methane and Ethane on MSC-30, ZTC and CNS-201

	MSC-30	ZTC	CNS-201
krypton	0.062	0.058	0.085
methane	0.076	0.072	0.097
ethane	0.069	0.066	0.080
mean and spread	0.069±10%	0.065±11%	0.087±11%

The validity of Equation S9 is also investigated by comparing $\frac{(-\Delta H_{ads})}{T_c}$ as a function of fractional occupancy on MSC-30 and ZTC (based on the availability of high pressure isosteric enthalpy of adsorption data at corresponding temperatures). On MSC-30, the $\frac{(-\Delta H_{ads})}{T_c}$ values approximately track one another as they decrease monotonically with fractional occupancy due to binding-site heterogeneity (Figure S4). On ZTC, methane and krypton exhibit anomalous surface thermodynamics at temperatures below T_0 due to cooperative adsorbate-adsorbate interactions. This leads to $\frac{(-\Delta H_{ads})}{T_c}$ values that initially increase with fractional occupancy, but nonetheless approximately track one another (Figure S5) due to the considerations explained in Sections 4.2 (Chapter 8) and S7 (Chapter 9). Additional discrepancies may result from uncertainty in the n_{max} parameter.

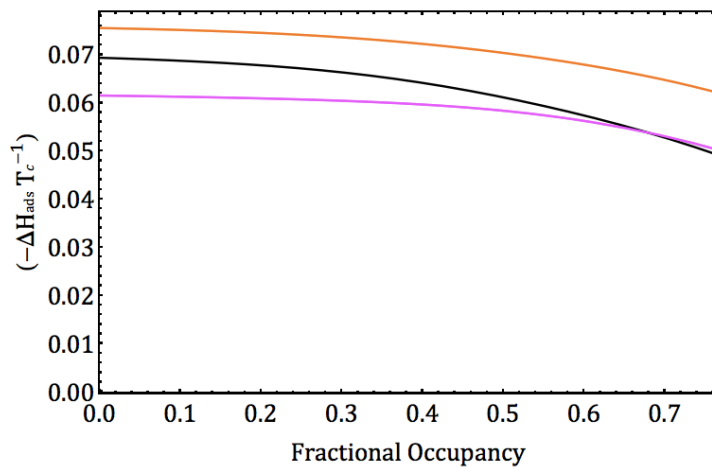


Figure S4. Comparison of $\frac{(-\Delta H_{ads})}{T_c}$ of methane (orange), krypton (purple), and ethane (black) on MSC-30 at a reduced temperature of 1.25.

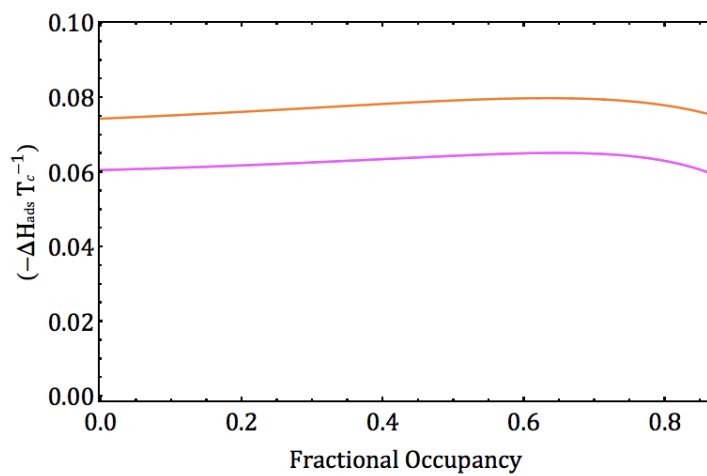


Figure S5. Comparison of $\frac{(-\Delta H_{ads})}{T_c}$ of methane (orange) and krypton (purple) on ZTC at a reduced temperature of 1.25.

S6. Generalizing the Proportionality

Between ΔH_{ads} and T_c to NonIdeal Gases

The molar enthalpy of an ideal gas depends solely on the temperature. This, along with the assumptions in Section 4.1 of Chapter 8, allows for a constant $\frac{-\Delta H_{ads}}{T}$ for multiple gases individually adsorbed on a single adsorbent at a fixed reduced temperature. The enthalpy of a nonideal gas, however, depends on pressure and volume as well as temperature, as illustrated by the case of a van der Waals gas (H_{vdW})

$$H_{vdW} = \frac{3}{2} N k_B T - \frac{N^2 a}{V} + PV \quad (S10)$$

where N is the number of gas molecules, k_B is Boltzmann's constant, T is the temperature, P is the pressure, V is the volume of the system, and a and b are the van der Waals parameters. Expressed as a function of T^R , P^R , and V^R :

$$H_{vdW} = \frac{a}{b} \left[\frac{4NT^R}{9} - \frac{N}{3V^R} + \frac{P^R V^R N}{27} \right] \quad (S11)$$

The van der Waals critical temperature, $T_c = \frac{8a}{27bNk_B}$, can also be included giving:

$$H_{vdW} = \left(\frac{27T_c N k_B}{8} \right) \left[\frac{4NT^R}{9} - \frac{N}{3V^R} + \frac{P^R V^R N}{27} \right] \quad (S12)$$

The gas-phase molar enthalpy (H_g) of a van der Waals gas is therefore proportional to the critical temperature and otherwise depends only on the reduced quantities as:

$$H_g \propto T_c f(T^R, P^R, V^R) \quad (S13)$$

Furthermore, we assume that the adsorbed-phase molar enthalpy (H_a) is proportional to the critical temperature, and otherwise depends only on the fractional occupancy and reduced quantities (as empirically supported by the data in Figure 3 of Chapter 8).

$$H_a \propto T_c f(\theta, T^R, P^R, V^R) \quad (\text{S14})$$

Since the isosteric enthalpy of adsorption is the difference between the gas-phase and adsorbed-phase enthalpies at constant coverage, T_c can be factored out of both:

$$\Delta H_{ads} \propto T_c [f(T^R, P^R, V^R) - f(\theta, T^R, P^R, V^R)] \quad (\text{S15})$$

The isosteric enthalpy of adsorption of a van der Waals gas is therefore proportional to its critical temperature, and otherwise depends only on the fractional occupancy and reduced quantities.

S7. Assumption that the Contributions of Adsorbate-Adsorbate Interactions to ΔH_{ads} are Proportional to $f(\theta)T_c$

Methane and krypton adsorption on ZTC exhibit anomalous surface thermodynamics where the isosteric heats of adsorption increase with coverage.^{16,17} This results from adsorbate-adsorbate interactions that are enhanced by the surface nanostructure. We have previously provided both enthalpic and entropic evidence of adsorbed-phase clustering on ZTC.^{9,17} In this work we draw a connection between the adsorbed-phase clustering and the Ising model by analyzing the temperature dependence of the clustering as an unmixing phase transition. The applicability of this model is supported by considerations of the adsorbed-phase heat capacity (Figure 5 of Chapter 8) and the general temperature dependence of the effect (Figure 6 of Chapter 8). To use the Ising model, we assume the critical temperature of the unmixing phase

transition (T_θ) is proportional to the Lennard-Jones interaction potential (ϵ) of the adsorbate, and hence proportional to the critical temperature of the adsorbate (T_c).¹⁸ We define a reduced phase-transition critical temperature (T_o^R) such that

$$T_o^R = \frac{T}{T_o} \quad (\text{S16})$$

By the transitive property

$$T_o^R \propto T^R \quad (\text{S17})$$

For $T_o^R < 1$, unmixing occurs, and the adsorbate-vacancy binary solid solution separates into a vacancy-rich α' phase and an adsorbate-rich α'' phase. The adsorbate concentration in each phase, $c_{\alpha'}$ and $c_{\alpha''}$, respectively, depends on T_o^R . The relative phase fraction of the α'' phase

($F_{\alpha''}$) is given by the lever rule:

$$F_{\alpha''} = \frac{\theta + c_{\alpha''} - 1}{2c_{\alpha''} - 1} \quad (\text{S18})$$

The adsorbate-adsorbate interaction energy is predominantly from the adsorbate-rich α'' phase. Under the assumption of random ordering (the point approximation), the average adsorbate-adsorbate energy per molecule in the α'' phase, $U_{\alpha''}$, is

$$U_{\alpha''} = \frac{z\epsilon c_{\alpha''}}{2} \quad (\text{S19})$$

where z is the coordination number. The overall adsorbate-adsorbate energy per molecule, U_{avg} in both phases is given by a weighted average of the mean adsorbate energy in each phase and the fraction of adsorbate molecules in each phase

$$U_{avg} = \frac{F_{\alpha'} c_{\alpha'} U_{\alpha'} + F_{\alpha''} c_{\alpha''} U_{\alpha''}}{\theta} \quad (\text{S20})$$

where the energy of the vacancy-rich phase, $U_{\alpha'}$, is assumed to be zero. By substitution we arrive at a general expression to model U_{avg} .

$$U_{avg} = \left(\frac{z\epsilon c_{\alpha'}^2}{2} \right) \left(\frac{\theta + c_{\alpha'} - 1}{2c_{\alpha'} - 1} \right) \left(\frac{1}{\theta} \right) \quad (S21)$$

For a fixed reduced temperature, $c_{\alpha'}$ is a constant. The coordination number, z , is also assumed to be a constant. Equation S21 is thus the product of a function proportional to ϵ and a function $f(\theta)$ that only varies with θ . Notably this equation displays the expected qualitative behaviors, increasing as a function of fractional occupancy at low coverage and leveling off at high coverage. We may make the assumption that ϵ is proportional to T_c ¹⁸ leaving an equation that only varies with $f(\theta)T_c$.

S8. Justification for the Law of Corresponding States in Bulk Gases

The Law of Corresponding States in bulk fluids is well established and can be readily understood by examining the van der Waals equation of state:

$$P = \frac{RT}{V-b} - \frac{a}{V^2} \quad (S22)$$

Here, P is pressure, T is temperature, V is volume, R is the gas constant, and a and b are the van der Waals parameters (unique for each gas). By substituting in the reduced temperature, reduced pressure and reduced volume:

$$P^*P_c = \frac{RT^*T_c}{V^*V_c - b} - \frac{a}{V^*V_c} \quad (S23)$$

The critical quantities in terms of the van der Waals parameters (a and b)¹⁹ are

$$T_c = \frac{8a}{27Rb} \quad (\text{S24})$$

$$P_c = \frac{a}{27b^2} \quad (\text{S25})$$

$$V_c = 3b \quad (\text{S26})$$

Substituting these critical quantities into Equation S23:

$$P^R = \frac{8T^R}{3V^{R-1}} - \frac{3}{V^{R^2}} \quad (\text{S27})$$

Equation 11 depends only on reduced quantities, which are by definition identical for all gases at corresponding conditions, thus providing a basis for the Law of Corresponding States in bulk fluids.

S9. Additional Data Compared with Law of Corresponding States for Physisorption

Using experimental physisorption data published elsewhere, the Law of Corresponding States for physisorption is illustrated on three additional adsorbents, each representing a unique class of materials. These examples showcase the importance of the adsorbate molecular volume. Two plots are shown for each adsorbent, the first comparing excess adsorption at corresponding conditions and the second comparing excess occupancies at corresponding conditions. In each case, excess occupancies at corresponding conditions have better agreement than excess adsorption at corresponding conditions. This is especially pronounced for adsorbates that have very different liquid molar volumes (e.g. argon and cyclohexane).

Agot Grade Artificial Nuclear Graphite²⁰

In Figure S6, argon and nitrogen adsorption isotherms on highly pure graphite are compared at a reduced temperature of 0.6 ± 0.01 . Argon and nitrogen have similar van der Waals molar volumes of 0.03201 and 0.0387 L mol⁻¹ respectively. Thus switching from a

comparison of excess adsorption to excess occupancy only minimally improves the agreement between the corresponding isotherms.

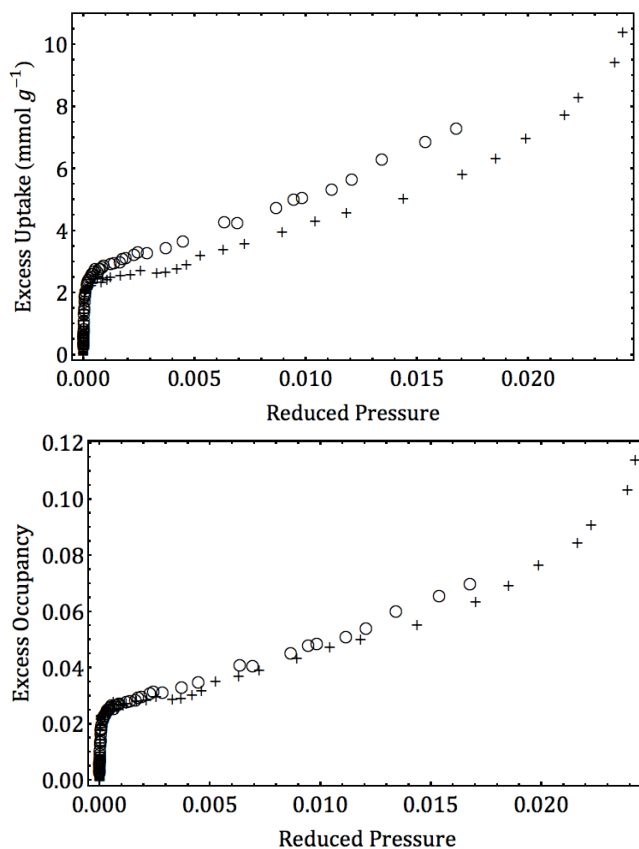


Figure S6. Comparison of excess adsorption (top) and excess occupancy (bottom) of argon (circles) and nitrogen (+) adsorption on Agot grade artificial nuclear graphite at corresponding conditions ($T^R = 0.6 \pm 0.01$).²⁰

Ni(bodc)(ted)_{0.5} Metal-Organic Framework²¹

In Figure S7, argon and cyclohexane adsorption isotherms on Ni(bodc)(ted)_{0.5} are compared at a reduced temperature of 0.57 ± 0.01 . Argon and cyclohexane have dissimilar van der Waals molar volumes of 0.03201 and 0.1424 L mol⁻¹ respectively. This leads to large

discrepancies when comparing excess adsorption that are resolved by comparing excess occupancy.

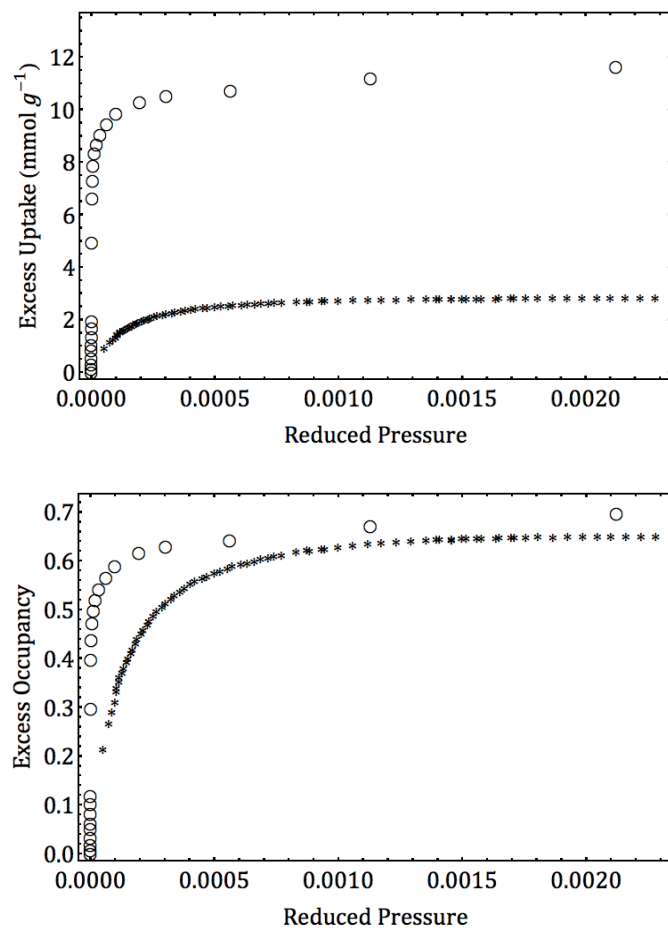


Figure S7. Comparison excess adsorption (top) and excess occupancy (bottom) of argon (circles) and cyclohexane (*) adsorption on $[\text{Ni}(\text{bodc})(\text{ted})_{0.5}]$ at corresponding conditions ($T^{\text{R}} = 0.57 \pm 0.01$).²¹

Zeolite NaX²²

In Figure S8, carbon dioxide, ethane, and sulfur hexafluoride adsorption isotherms on zeolite NaX are compared at a reduced temperature of 0.94 ± 0.02 . The van der Waals molar volumes of carbon dioxide, ethane, and sulfur hexafluoride are 0.04267, 0.0638, and 0.08786 L mol⁻¹, respectively. Comparing excess occupancies rather than excess adsorption improves the

agreement of the isotherms. It is notable that all three gases have similar critical temperatures of 304, 305, and 319 K respectively, and yet the differences in the van der Waals molar volumes yield significant discrepancies when comparing excess adsorption.

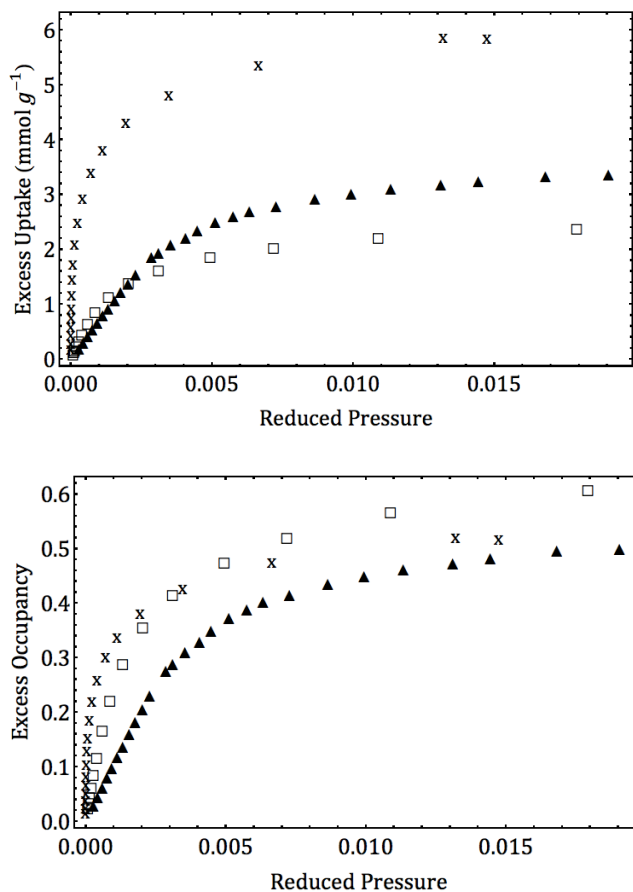


Figure S8. Comparison of excess adsorption (top) and excess occupancy (bottom) of carbon dioxide (x), ethane (triangles), and sulfur hexafluoride (squares) adsorption on zeolite NaX at corresponding conditions ($T^R = 0.94 \pm 0.02$).²²

S10. Heat of Liquefaction vs. Critical Temperature

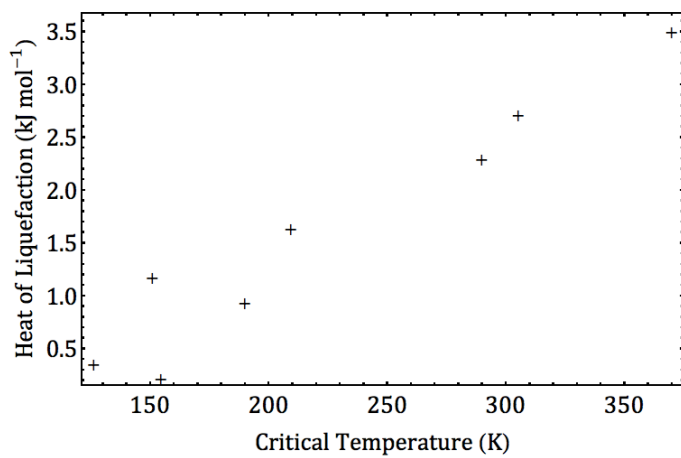


Figure S9. Plotting the heat of liquefaction as a function of critical temperature for moderately-sized classical gases shows an approximately linear correlation.⁸

References:

1. Tarazona, P.; Marconi, U. M. B.; Evans, R. Phase-Equilibria of Fluid Interfaces and Confined Fluids - Nonlocal Versus Local Density Functionals. *Mol. Phys.* **1987**, *60*, 573-595.
2. Dumas, J. B. A Method of Estimating Nitrogen in Organic Material. *Ann. Chim. Phys.* **1833**, *58*, 171-173.
3. Stadie, N. P.; Vajo, J. J.; Cumberland, R. W.; Wilson, A. A.; Ahn, C. C.; Fultz, B. Zeolite-Templated Carbon Materials for High-Pressure Hydrogen Storage. *Langmuir* **2012**, *28*, 10057-10063.
4. Dubinin, M. M.; Radushkevich, L. V. Equation of the Characteristic Curve of Activated Charcoal. *Proc. Acad. Sci. USSR, Phys. Chem. Sect.* **1947**, *55*, 331-337.
5. Nguyen, C.; Do, D. D. The Dubinin-Radushkevich Equation and the Underlying Microscopic Adsorption Description. *Carbon* **2001**, *39*, 1327-1336.
6. Kyotani, T.; Nagai, T.; Inoue, S.; Tomita, A. Formation of New Type of Porous Carbon by Carbonization in Zeolite Nanochannels. *Chem. Mater.* **1997**, *9*, 609-615.
7. Nishihara, H.; Hou, P.-X.; Li, L.-X.; Ito, M.; Uchiyama, M.; Kaburagi, T.; Ikura, A.; Katamura, J.; Kawarada, T.; Mizuuchi, K.; Kyotani, T. High-Pressure Hydrogen Storage in Zeolite-Templated Carbon. *J. Phys. Chem. C* **2009**, *113*, 3189-3196.
8. Lemmon, E. W.; Huber, M. L.; McLinden, M. O. *NIST Standard Reference Database 23: Reference Fluid Thermodynamic and Transport Properties-REFPROP*, version 8.0; National Institute of Standards and Technology: Gaithersburg, MD, 2007; CD-ROM.
9. Stadie, N. P.; Murialdo, M.; Ahn, C. C.; Fultz, B. Unusual Entropy of Adsorbed Methane on Zeolite-Templated Carbon. *J. Phys. Chem. C* **2015**, *119*, 26409-26421.
10. Hildebrand, J. H. The Entropy of Vaporization as a Means of Distinguishing Normal Liquids. *J. Am. Chem. Soc.* **1915**, *37*, 970-978.
11. Hildebrand, J. H. Liquid Structure and Entropy of Vaporization. *J. Chem. Phys.* **1939**, *7*, 233-235.
12. Green, J. A.; Irudayam, S. J.; Henschman, R. H. Molecular Interpretation of Trouton's and Hildebrand's Rules for the Entropy of Vaporization of a Liquid. *J. Chem. Thermodyn.* **2011**, *43*, 868-872.
13. London, F. The General Theory of Molecular Forces. *Trans. Faraday Soc.* **1937**, *33*, 8-26.
14. Bretsznajder, S. *International Series of Monographs in Chemical Engineering: Prediction of Transport and Other Physical Properties of Fluids*; Pergamon Press: New York, 1971.
15. Rice, J. E.; Taylor, P. R.; Lee, T. J.; Almlöf, J. The Determination of Accurate Dipole Polarizabilities Alpha and Gamma for the Noble-Gases. *J. Chem. Phys.* **1991**, *94*, 4972-4979.
16. Stadie, N. P.; Murialdo, M.; Ahn, C. C.; Fultz, B. Anomalous Isothermic Enthalpy of Adsorption of Methane on Zeolite-Templated Carbon. *J. Am. Chem. Soc.* **2013**, *135*, 990-993.

17. Murialdo, M.; Stadie, N. P.; Ahn, C. C.; Fultz, B. Krypton Adsorption on Zeolite-Templated Carbon and Anomalous Surface Thermodynamics. *Langmuir* **2015**, *31*, 7991-7998.
18. Evans, G. J. Cooperative Molecular Behavior and Field Effects on Liquids: Experimental Considerations. In *Dynamical Processes in Condensed Matter*; Evans, M. W., Ed.; John Wiley and Sons: New York, 1985; 293-376.
19. Haentzschel, E. The Calculation of the A and B Constants of van der Waals's Equation from Critical Values. *Ann. Phys.* **1905**, *16*, 565-573.
20. Banaresmunoz, M. A.; Gonzalez, L. V. F.; Llorenta, J. M. M. Adsorption-Isotherms of Nitrogen and Argon on an Agot Grade Artificial Nuclear Graphite at 77-K and 90-K. *Carbon* **1987**, *25*, 603-608.
21. Li, K. H.; Lee, J.; Olson, D. H.; Emge, T. J.; Bi, W. H.; Eibling, M. J.; Li, J. Unique Gas and Hydrocarbon Adsorption in a Highly Porous Metal-Organic Framework Made of Extended Aliphatic Ligands. *Chem. Commun.* **2008**, *46*, 6123-6125.
22. Siperstein, F. R.; Myers, A. L. Mixed-Gas Adsorption. *Aiche J.* **2001**, *47*, 1141-1159.